

Precision measurement of the $^{43}\text{Ca}^+$ nuclear magnetic moment

R. K. Hanley,¹ D. T. C. Allcock,^{1,2} T. P. Harty,¹ M. A. Sepiol,¹ and D. M. Lucas^{1,*}

¹*Department of Physics, University of Oxford, Clarendon Laboratory, Parks Road, Oxford OX1 3PU, U.K.*

²*Department of Physics, University of Oregon, Eugene, OR, USA*

(Dated: September 1, 2021)

We report precision measurements of the nuclear magnetic moment of $^{43}\text{Ca}^+$, made by microwave spectroscopy of the $4s\ ^2S_{1/2}\ |F=4, M=0\rangle \rightarrow |F=3, M=1\rangle$ ground level hyperfine clock transition at a magnetic field of $\approx 146\text{ G}$, using a single laser-cooled ion in a Paul trap. We measure a clock transition frequency of $f = 3\,199\,941\,076.920(46)\text{ Hz}$, from which we determine $\mu_I/\mu_N = -1.315350(9)(1)$, where the uncertainty (9) arises from uncertainty in the hyperfine A constant, and the (1) arises from the uncertainty in our measurement. This measurement is not corrected for diamagnetic shielding due to the bound electrons. We make a second measurement which is less precise but agrees with the first. We use our μ_I value, in combination with previous NMR results, to extract the change in shielding constant of calcium ions due to solvation in D_2O : $\Delta\sigma = -0.00022(1)$.

The favourable scaling laws of bound-state QED (BSQED) effects with proton number Z have made highly-charged hydrogen- and lithium-like ions ideal probes of fundamental theories of atomic constituents, leading to significant theoretical [1] and experimental [2–5] attention. An overview of tests of BSQED are discussed in detail in recent reviews by Kozlov *et al.* [6] and Indelicato [7]. However, as with the proton-size puzzle preventing further improvements in tests of QED [8–10], progress in stringent tests of BSQED is limited by our understanding of finite nuclear-size effects [11]. The dominant source of error [12] is the Bohr-Weisskopf effect [13, 14], which describes the spatial distribution of the nuclear magnetisation. Typically one relies upon measured nuclear magnetic moments (μ_I) to infer the theoretical Bohr-Weisskopf correction. The precision at which one can test BSQED thus relies upon the precision of the known μ_I . The importance of such measurements is exemplified by the ‘Bismuth Hyperfine Puzzle’, where an incorrect measurement of μ_I in ^{209}Bi resulted in a 7σ difference between experimental and theoretical predictions [11, 15, 16].

In addition to tests of BSQED, highly-charged ions have also been used to probe nuclear structure [17–19]. Of particular interest are ions with magic numbers of nucleons [20]. Recently there has been significant theoretical [21–27] and experimental attention [28–32] given to the calcium isotopic chain as there exist two naturally-occurring doubly-magic isotopes, ^{40}Ca and ^{48}Ca . The properties of the calcium isotopic chain can reveal new aspects of nuclear forces, such as three-body contributions [33] and the appearance of new magic numbers at extreme neutron-to-proton ratios [34–37]. Precise spectroscopic measurements of μ_I are again critical, as typically one uses a reference nucleus of the same element to deduce unknown properties of other isotopes [32].

The interaction of an atom with electronic angular momentum \mathbf{J} and nuclear spin \mathbf{I} , and a static magnetic field

\mathbf{B} is described to good approximation by the Hamiltonian [38]

$$\begin{aligned} H &= hA\mathbf{I} \cdot \mathbf{J} - (\boldsymbol{\mu}_J + \boldsymbol{\mu}_I) \cdot \mathbf{B}, \\ &= hA\mathbf{I} \cdot \mathbf{J} + (g_J\mu_B\mathbf{J} - g_I\mu_N\mathbf{I}) \cdot \mathbf{B}, \end{aligned} \quad (1)$$

where h is Planck’s constant, A is the magnetic dipole hyperfine interaction constant, g_J and g_I are the electronic and nuclear g -factors, and μ_B and μ_N are the Bohr and nuclear magnetons. Note that the apparent sign change arises from the conventional definitions of $\boldsymbol{\mu}_J$ and $\boldsymbol{\mu}_I$. The first term describes the magnetic dipole interaction between the nucleus and bound electrons, and the second and third terms describe the Zeeman interaction between the static magnetic field and the electronic and nuclear magnetic moments respectively. The energy eigenstates of this Hamiltonian, in general, must be numerically calculated. However, for the case where $J = 1/2$, the eigenstate energies are given analytically by the Breit-Rabi formula [38, 39]

$$\begin{aligned} E_{\pm}(B, M) &= -\frac{E_{\text{hfs}}}{2(2I+1)} - g_I\mu_N BM \\ &\quad \pm \frac{E_{\text{hfs}}}{2} \sqrt{1 + \frac{4\chi BM}{2I+1} + \chi^2 B^2}, \end{aligned} \quad (2)$$

where $M = M_I + M_J$ is the magnetic quantum number, $E_{\text{hfs}} = hA(I+1/2)$ is the zero-field energy splitting between the two hyperfine manifolds, and $\chi = (g_I\mu_N + g_J\mu_B)/E_{\text{hfs}}$. The Breit-Rabi formula highlights that the transition frequency between states in the $J = 1/2$ manifold depends upon three intrinsic properties of the atomic ground level; namely the zero-field hyperfine splitting, and the nuclear and electronic magnetic moments. Spectroscopy of ground-level hyperfine structure is therefore an excellent technique to test physical theories of atomic constituents.

Many spectroscopic techniques have been used to determine these constants. The earliest techniques used spectroscopy in thermal atomic beams (see Arimondo *et al.* [40] for a detailed review), or nuclear-magnetic-resonance (NMR) spectroscopy. The accuracy of NMR

* david.lucas@physics.ox.ac.uk

μ_I/μ_N	Environment	Reference
-1.3152(2)	Liquid NMR, Ca^{2+}	[50]
-1.315645(7)	Liquid NMR, Ca^{2+}	[51]
-1.31537(60)	Atomic vapour, Ca	[52]
-1.315350(9)(1)	Single trapped ion, Ca^+	This work
-1.315349(9)(4)	Single trapped ion, Ca^+	This work

TABLE I. Measurements of the nuclear magnetic moment of ^{43}Ca in units of μ_N , and the environment in which they were measured. Note that all of these measurements are uncorrected for diamagnetic shielding due to bound electrons, and the NMR measurements are uncorrected for chemical shifts. With respect to the results obtained in this work, the two uncertainties correspond to the contribution due to the uncertainty in the ground-level hyperfine splitting E_{hfs} measured by Arbes *et al.* [47], and the uncertainty in our measurements respectively.

measurements is limited by the systematic error caused by the ‘chemical shift’ [41–43], which describes the magnetic shielding of the target nucleus by the solution in which the atom is measured. The chemical shift is challenging to calculate [43] and has led to significant disagreements between theory and experiment [16]. The advent of ion trapping extended the possibility of measurements to ions, consequently enhancing the achievable precision due to the ability to confine ions to a small region of free space which minimises effects such as magnetic field inhomogeneities, removes chemical shifts, and provides extremely long coherence times [44–46].

^{43}Ca is the only naturally occurring calcium isotope with non-zero nuclear spin ($I = 7/2$), making it an ideal reference nucleus. All three of the relevant atomic constants have been previously measured. Arbes *et al.* [47] measured $E_{\text{hfs}} = 3\,225\,608\,286.4(3)$ Hz using double-resonance spectroscopy of $^{43}\text{Ca}^+$ ions in a Paul trap, and Tommaseo *et al.* [48] measured $g_J = 2.002\,256\,64(9)$ using double-resonance spectroscopy of $^{40}\text{Ca}^+$ ions in a Penning trap. One would expect the isotopic dependence of g_J to be smaller than the experimental measurement uncertainty, based upon similar measurements using Ba^+ isotopes [49]. There exist three previous measurements of μ_I for ^{43}Ca which are summarised in table I. Two measurements were made using NMR of liquid Ca salts [50, 51], and the other by spectroscopy in an atomic vapour [52].

This paper details two precision measurements of μ_I using a single $^{43}\text{Ca}^+$ ion held in a surface-electrode Paul trap with integrated microwave circuitry [53]. Ramsey spectroscopy [54] was performed on the $|F = 4, M = 0\rangle \rightarrow |F = 3, M = 1\rangle$ clock transition [55], at $B = 146.094$ G, where the coherence time is of the order of minutes [56] due to the lack of first-order magnetic field sensitivity. The two measurements were taken nine months apart in the same apparatus, and used either the time or frequency variants of Ramsey spectroscopy. The remainder of this paper is structured as follows. We ini-

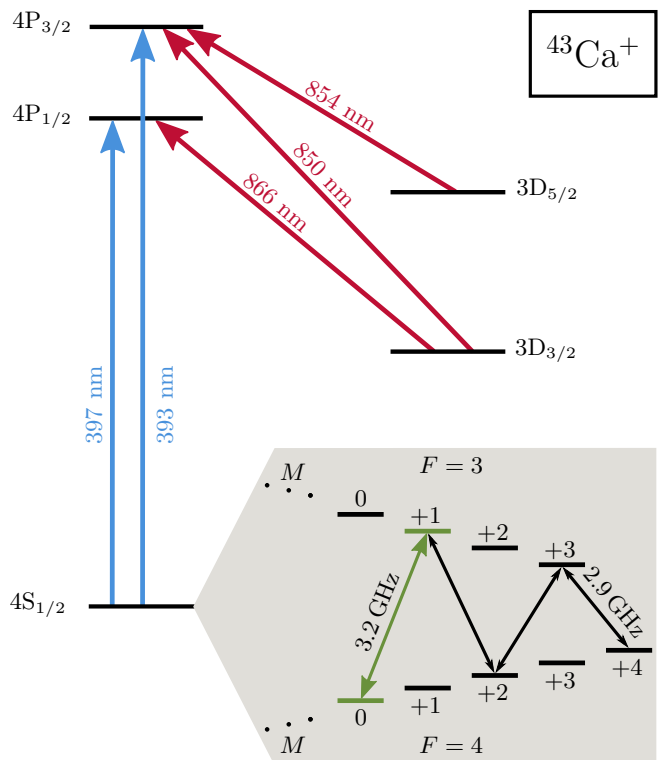


FIG. 1. Energy level diagram of $^{43}\text{Ca}^+$ at $B = 146.094$ G showing the relevant states for laser cooling, state preparation, and readout. The lower panel shows the hyperfine structure of the $4S_{1/2}$ state. The green states show the clock transition used for the measurements in this work, and the thin black arrows show the transitions used for state preparation and readout.

tially describe the experimental apparatus and measurement techniques used, before analysing in detail sources of systematic uncertainty in our measurement. We then report the systematic-corrected measurement of μ_I , and compare to previous measurements. We estimate the diamagnetic-corrected nuclear moment using published calculations of the shielding constants for Ca [57] and Ca^{2+} [58]. From our measurement, and previous NMR spectroscopy [51], we extract the change in shielding constant of between a free Ca^+ ion and Ca^{2+} ions in D_2O solution.

A single $^{43}\text{Ca}^+$ ion was loaded into a surface trap [53] from a 12% isotopically enriched calcium source using isotope-selective photoionization [59]. The ion was Doppler cooled on the 397 nm $4S_{1/2} \rightarrow 4P_{1/2}$ transition, and repumped by an 866 nm laser to close the cooling cycle (see figure 1). The RF trapping field was driven at 38.7 MHz, and the radial secular frequency was varied between 2 MHz and 4 MHz. The axial frequency was 0.5 MHz. A static magnetic field was provided by current flowing through two coils external to the vacuum chamber. Transitions between energy levels in the ground-state hyperfine manifolds were driven directly by the magnetic field generated from a current applied to one

of the trap's integrated microwave electrodes. The microwaves were synthesized using a commercial microwave synthesizer phase-locked to a rubidium frequency standard (RbFS [60]). To ensure an accurate absolute frequency measurement, the phase difference between the RbFS and a GPS-disciplined oscillator (GPSDO [61]) was measured for a period of 12 hrs directly after the clock transition frequency measurements. At this time interval, the GPSDO has a frequency stability of 1.16×10^{-12} .

Additional lasers were used for state preparation and readout [56, 62]. We first optically pumped the ion to the $|F = 4, M = 4\rangle$ state using circularly-polarized 397 nm light, after which the ion was prepared into the $|F = 3, M = 1\rangle$ state via a series of microwave π pulses (see figure 1). After experiments on the clock transition, microwave π pulses transferred population in the $|F = 3, M = 1\rangle$ state back to the $|F = 4, M = 4\rangle$ state. Population in the $|F = 4, M = 4\rangle$ state was then shelved in the metastable $3D_{5/2}$ level by a series of 393 nm and 850 nm pulses (see [62] for further details). The Doppler cooling beams were then applied and the state of the ion inferred by the absence or presence of ion fluorescence. The ion was repumped to the ground level using an 854 nm pulse.

The applied static magnetic field was measured using Rabi spectroscopy on the stretch $|F = 4, M = 4\rangle \rightarrow |F = 3, M = 3\rangle$ transition. This transition is first-order sensitive to the applied magnetic field, with a transition frequency sensitivity of $df/dB = -2.36$ MHz/G. After optical pumping into the $|F = 4, M = 4\rangle$ state, a microwave π -pulse was applied and the probability of remaining in the $|F = 4, M = 4\rangle$ state was measured using electron shelving [56, 62]. The pulse π -time was 22.2 μ s, leading to a transition FWHM of 36 kHz. The coil current was then adjusted to ensure agreement between the measured stretch transition frequency and that predicted by the Breit-Rabi formula at the clock field of 146.094 G. The experimental uncertainties in E_{hfs} , g_I , and g_J contribute a systematic frequency shift of the stretch transition which is three orders of magnitude smaller than the systematic shift induced by magnetic field fluctuations. This procedure enabled calibration of the static magnetic field to an accuracy of ≈ 1 mG.

Ramsey spectroscopy [54] (see figure 2(a)) was used to measure the clock transition frequency (f), as the long coherence time facilitates large Ramsey delays (τ_R) and hence enhanced precision. The two measurements of the clock transition frequency used differing variants of Ramsey spectroscopy. The first measurement consisted of Ramsey interferometry using a fixed microwave frequency ($f_{\mu\text{W}}$) and a variable Ramsey delay, whilst the second measurement consisted of varying the microwave frequency with a fixed Ramsey delay. Using two variants of Ramsey spectroscopy gives us increased confidence in our evaluation of systematic errors.

The first measurement of the clock qubit transition frequency was performed as follows. The magnetic field was set to 146.094 G using the stretch transition

$|F = 4, M = 4\rangle \rightarrow |F = 3, M = 3\rangle$ spectroscopy method outlined previously. The ion was then prepared in the $|F = 3, M = 1\rangle$ state via a series of microwave transfer pulses (see figure 1). A pair of $\pi/2$ -pulses was subsequently applied at a fixed frequency of $f_{\mu\text{W}}$ near 3.199 941 070 GHz, with a variable Ramsey delay $\tau_R = 0.1 \text{ s} \rightarrow 1 \text{ s}$. We inferred a fractional frequency deviation between the RbFS and the GPSDO of $f_{\text{RbFS}}/f_{\text{GPSDO}} = 3.22(2) \times 10^{-10}$, corresponding to a systematic shift of 1.030(8) Hz of the measured clock transition frequency. A typical Ramsey spectroscopy signal of the clock transition is shown in figure 2(b). The solid line is a fit to the data using an analytical expression for the propagator of a Ramsey interferometry sequence, where the only free parameters were the frequency offset and an amplitude scale factor to account for imperfect state readout. The lower figures show a plot of the normalised residuals R_ν [63], defined as the residuals between the data and the fit, normalised to their respective uncertainty.

Figure 2(c) shows the measured clock transition frequency as a function of applied trapping RF power (P_{RF}). Currents flowing in the RF trapping electrodes generate oscillating magnetic fields at the RF drive frequency (38.7 MHz). These oscillating magnetic fields off-resonantly couple states within each hyperfine manifold, which are separated by approximately 50 MHz, resulting in a systematic shift of the clock transition frequency. The unperturbed transition frequency in the absence of the AC Zeeman shift caused by the trapping RF is therefore determined from the intercept of the straight-line fit in figure 2(c). The figure shows the frequency shift is of the order of several Hz. This is larger than one might expect in comparison to an ion frequency standard [64], as ion frequency standards typically use a Paul trap where the RF electrodes are symmetric about the ion and therefore the generated magnetic fields are nulled at the ion. However, in a surface trap the null is in the plane of the trap and therefore the magnitude of cancellation is greatly reduced. The residuals show excellent agreement between theory and experiment; however they also highlight an outlier point at $P_{\text{RF}} \approx 500$ mW. This point lies above the fitted line by ≈ 50 mHz, and may indicate drifts in systematic shifts over the timescale of a full data collection cycle; it is consistent with our systematic uncertainty (see below).

The second measurement of the clock transition frequency was performed nine months later in the same apparatus. The clock transition frequency was measured as a function of applied magnetic field about 146.094 G, using a fixed trap RF power. The ion was prepared in the $|F = 3, M = 1\rangle$ state, after which a pair of $\pi/2$ -pulses was applied at a variable detuning $\Delta f_{\mu\text{W}}$ about the clock transition frequency with a fixed Ramsey delay. Figure 3 shows a typical Ramsey spectroscopy signal of the clock transition at a static magnetic field offset from the clock field $\Delta B = 100$ mG using Ramsey delays $\tau_R = 1.05$ ms (a) and $\tau_R = 24.93$ ms (b), identifying a frequency shift of 11.34(8) Hz. The short Ramsey delay was used to iden-

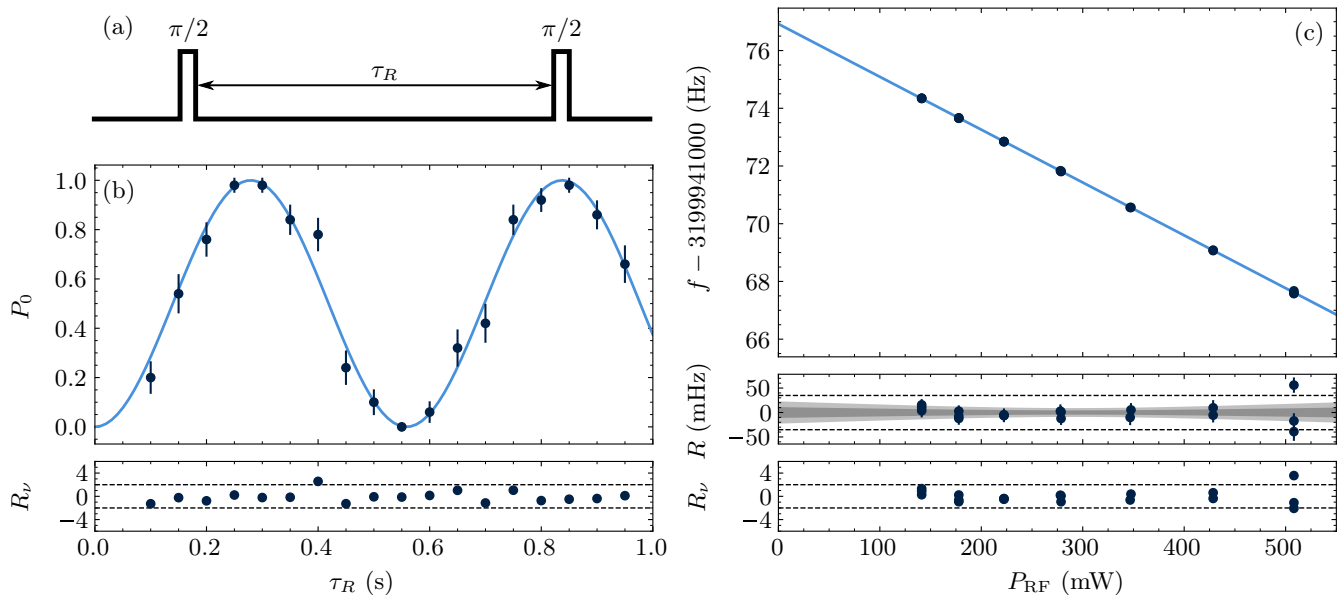


FIG. 2. (a) Pulse sequence used for Ramsey interferometry. The ion is first prepared in the $|F = 3, M = 1\rangle$ state before applying a pair of $\pi/2$ -pulses of duration $20.9\mu\text{s}$, at a frequency ($f_{\mu\text{W}}$) and separated by a Ramsey delay τ_R . The ion's resulting state was subsequently measured using electron shelving. Figure (b) shows a typical Ramsey spectroscopy signal on the clock transition at a trap RF power (P_{RF}) of 279 mW , driven with a $\pi/2$ -pulse duration of $20.9\mu\text{s}$ and a microwave frequency of $f_{\mu\text{W}} = 3\,199\,941\,070\text{ Hz}$. The error bars are from quantum projection noise. The solid line is a fit to the data using an analytical expression for the propagator of a Ramsey interferometry sequence, where the free parameters are the frequency offset, $-1.791(12)\text{ Hz}$, and an amplitude scale factor. Figure (c) shows the measured clock transition frequency f as a function of applied trap RF power. The solid line is a weighted straight-line fit to the data. The lower figures show the residuals R , and the normalised residuals R_ν . Error bars represent the combined uncertainty from the Ramsey fit and from the digitisation error of the RF power meter. The smaller and larger shaded regions in the plot of residuals shows the 68% and 95% confidence intervals of the linear fit respectively, the dashed lines illustrate the $\pm 35\text{ mHz}$ total systematic uncertainty, and the dashed lines in the plot of the normalised residuals show $R_\nu = \pm 2$. We calculate the reduced chi-squared statistic to be $\chi_\nu^2 = 0.9$ (b) and $\chi_\nu^2 = 1.5$ (c). Note that the measured fractional frequency deviation between the RbFS and the GPSDO of $f_{\text{RbFS}}/f_{\text{GPSDO}} = 3.22(2) \times 10^{-10}$, corresponding to a systematic shift of $1.030(8)\text{ Hz}$ of the clock transition frequency, has been corrected in the data.

tify the central fringe, and the longer delay was used for the precision measurements. The solid line is once again a fit to the data using an analytical expression for the propagator of a Ramsey interferometry sequence, where the only free parameters were the frequency offset and an amplitude scale factor to account for imperfect state readout.

To determine the AC Zeeman shift of the clock transition frequency, we measured the clock transition frequency using Ramsey spectroscopy for a series of trap RF powers, as shown in figure 4(a). We observed a linear frequency shift as a function of trap RF power, corresponding to a systematic shift of $-5.050(120)\text{ Hz}$ at the RF power used during the subsequent experiments. We also measured a fractional frequency deviation between the RbFS and the GPSDO of $f_{\text{RbFS}}/f_{\text{GPSDO}} = 4.13(2) \times 10^{-10}$, corresponding to a systematic shift of $1.322(8)\text{ Hz}$ of the clock transition frequency. Figure 4(b) shows the measured clock transition frequency as a function of static magnetic field about 146.094 G , corrected for the systematic shifts discussed previously. The solid line is a fit to the data using the Breit-Rabi formula

from which we are able to extract the clock transition frequency and hence the nuclear magnetic moment. The only fit parameter was g_I , and values of E_{hfs} and g_J were taken from Arbes *et al.* [47] and Tommaseo *et al.* [48] respectively. The lower figure shows a plot of the normalised residuals, from which we calculate $\chi_\nu^2 = 1.3$, indicating an excellent agreement between theory and experiment.

The RF-induced AC Zeeman shift and the calibration of the RbFS were the major sources of systematic frequency shifts in these measurements. We now discuss the uncertainties in these shifts, and other sources of uncertainty (see table II).

The experimental uncertainty in the comparison of the RbFS with the GPSDO, together with the specified instability of the GPSDO, give a total uncertainty of 8 mHz in the RbFS calibration.

The largest uncertainty in correcting for the RF-induced AC Zeeman shift arises from any potential non-linearity in the RF power meter (Keysight V3500A) which was used to measure the applied trap RF power. By comparing the device to a precision power sensor

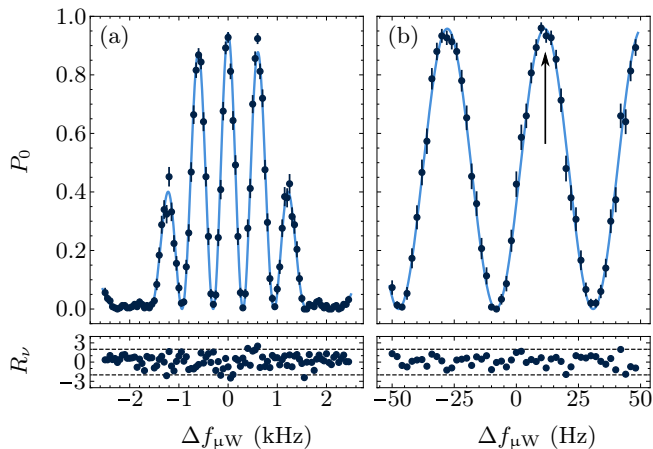


FIG. 3. Typical Ramsey spectroscopy signals on the clock transition using $\tau_R = 1.05$ ms (a) and $\tau_R = 24.93$ ms (b), a $\pi/2$ -pulse duration of $478.62 \mu\text{s}$, a microwave frequency $f_{\mu\text{W}} = 3\,199\,941\,071$ Hz, and static magnetic field offset from the clock field $\Delta B = 100$ mG. The error bars are from quantum projection noise. The vertical arrow in (b) indicates the central fringe. The solid line is a fit to the data using an analytical expression for the propagator of a Ramsey interferometry sequence, where the free parameters are the frequency offset and an amplitude scale factor. The lower figures show a plot of the normalised residuals R_ν . We calculate the reduced chi-squared statistic to be $\chi_\nu^2 = 1.04$ (a) and $\chi_\nu^2 = 0.84$ (b), and the dashed lines show $R_\nu = \pm 2$.

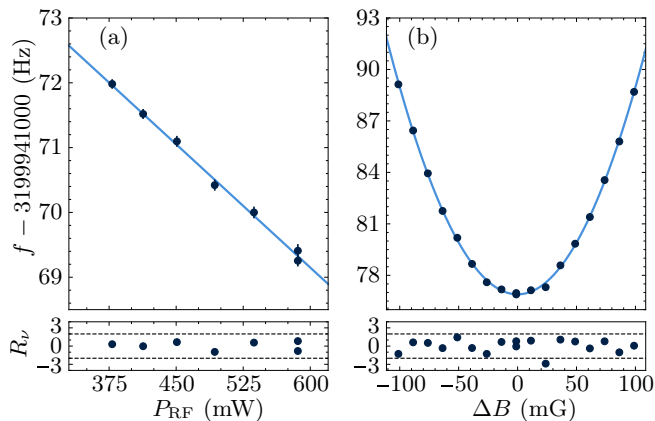


FIG. 4. (a) Clock-transition frequency shift as a function of applied trap RF power, where the solid line is a linear fit to the data. (b) Measured clock transition frequency as a function of applied static magnetic field offset from 146.094 G, measured at $P_{\text{RF}} = 392$ mW. The systematic shift due to the RF induced AC Zeeman shift ($-5.050(120)$ Hz) and the frequency deviation between the RbFS and the GPSDO ($1.322(8)$ Hz) have been applied to all points equally. The solid line is a fit to the experimental data using the Breit-Rabi formula with only g_I as a fitted parameter. The lower figures show the normalised residuals, from which we calculate $\chi_\nu^2 = 0.8$ (a) and $\chi_\nu^2 = 1.3$ (b) respectively. The dashed lines show $R_\nu = \pm 2$.

(Keysight N8481A), we measure any non-linearity to be < 0.015 dB over the range used in the experiment. We bound the uncertainty by re-fitting the data in figures 2(c) using a worst-case scenario in which the gradient is maximally affected. We find an upper limit on the uncertainty of the fitted intercept of ± 25 mHz. The power meter also has a ± 0.005 dB digitization error which, from the slope in figure 2(c), effectively gives a random frequency error between ± 3 mHz and ± 11 mHz for the range of powers used; this has been accounted for in the error bars in figure 2(c).

Drifts in RF power in the trap, relative to the measured input power, can occur for example due to variation in the step-up of the RF resonator. We can estimate such drifts by monitoring the ion's radial secular frequency, as $\omega_r \propto \sqrt{P_{\text{RF}}}$. We measured short-term variations in P_{RF} at the 0.05% level, and longer-term drift of 0.05%/hour [65]. As the data in figure 2(c) were taken mostly in time order, over ≈ 5 hours, a linear drift in time could systematically affect the fitted gradient. We determine the worst-case effect to be ± 10 mHz.

The RF-induced AC Zeeman shift is dependent upon the magnitude and polarization of the RF magnetic field at the ion position. Hence drifts of the ion's radial position during the experiments can lead to changes in the measured shift. To quantify this effect, we measured the clock transition frequency as a function of radial DC compensation fields E_x and E_y . We observe frequency shifts of $df/dE_x = 3.9(2)$ mHz/(V/m) and $df/dE_y = 2.34(7)$ mHz/(V/m) in the directions parallel and perpendicular to the trap surface respectively [66]. Experimentally, we observed that the micromotion compensation was stable to within ± 5 V/m and therefore assign an upper bound of ± 20 mHz to this systematic shift.

For larger excursions in ion position, such as could occur due to micromotion or thermal motion of the ion, we measure a quadratic dependence of the AC Zeeman shift on position [67], which will not average to zero. We observed intrinsic (uncompensatable) micromotion in the y direction of amplitude ≈ 20 nm, which leads to negligible shift. Based on the measured heating rate of the trap [68], the radial temperature of the ion is $T < 10$ mK after the longest (1 s) Ramsey delays, which would lead to a shift < 1 mHz.

Fluctuations in the static magnetic field B can cause frequency shifts in the measured clock transition frequency f . These enter at second order for the clock transition, for which $d^2 f/dB^2 = 2.416$ mHz/mG². The automated servo corrections to the static field which were applied during the experiment in figure 2 had an rms amplitude of 0.8 mG, implying a frequency shift of ≈ 1 mHz due to servo imprecision. A larger source of magnetic field noise is caused by 50 Hz mains power. We measured the effect of 50 Hz field modulation by performing Ramsey spectroscopy on the first-order sensitive $|F = 4, M = 4\rangle \rightarrow |F = 3, M = 3\rangle$ transition as a function of delay after the zero-crossing of the mains power cycle (line trigger). The measured transition fre-

Measurement	Source	Magnitude (mHz)	Uncertainty (mHz)
1	Rb frequency standard	1030	8
2	Rb frequency standard	1322	8
2	RF-induced AC Zeeman	5050	120
1, 2	RF power meter linearity	0	25
1, 2	RF power drift	0	10
1, 2	Ion position drift	0	20
1, 2	Ion position (thermal motion)	< 1	1
1, 2	Magnetic field (50 Hz)	11	8
1, 2	Magnetic field (DC error)	1	1
1, 2	Magnetic field (non-50 Hz)	< 0.1	0.1
1, 2	RF-induced AC Stark	< 0.01	0.01
1, 2	Blackbody AC Stark	< 0.01	0.01
1, 2	Second-order Doppler	< 0.001	0.001

TABLE II. Systematic frequency shifts of the measured clock transition frequency. The measurement column indicates to which measurement the shift applies, where the numbering follows the order of measurements presented in the main text. Note that for measurement 1, we extrapolate to zero RF-induced AC Zeeman shift; systematic uncertainty introduced by this extrapolation is accounted for by the values in the Table.

quency thus reveals the change in local magnetic field within each mains cycle. We measured an rms amplitude of 3(1) mG, which contributes a systematic shift of 11(8) mHz to the clock transition frequency. Field fluctuations incoherent with 50 Hz were bounded by comparing the measured spectral width of the stretch transition (whilst line-triggering to remove 50 Hz effects) to the theoretical width for our measured Rabi frequency. We were not able to measure a difference in spectral width within the experimental uncertainty of 0.6 kHz, which bounds shifts due to such field fluctuations to be < 0.1 mHz.

Residual electric fields at the ion can induce an AC Stark shift, of approximate magnitude 1×10^{-11} Hz/(V/m)² [69]. The intrinsic micromotion observed in the y direction implies an RF field of rms amplitude 400 V/m [70]. Hence the AC Stark shift due to trap fields is expected to be < 10 μ Hz. The rms electric field due to black body radiation at 300 K is 830 V/m [69], leading to a similar shift.

A second-order Doppler shift will also be present, due to the intrinsic micromotion and any thermal motion of the ion. The total shift is < 1 μ Hz.

We add the various systematic uncertainties in quadrature to obtain a total systematic uncertainty, which we add linearly to the statistical uncertainty for each measurement, to report both the clock transition frequency and the nuclear magnetic moment. We extract the clock transition frequency from the first measurement by determining the intercept in figure 2(c). This gives $f = 3199941076.920 \pm 0.011_{\text{stat}} \pm 0.035_{\text{syst}}$ Hz, which corresponds to a nuclear magnetic moment of $\mu_I/\mu_N = -1.315350(9)(1)$. We extract the clock transition frequency and the nuclear magnetic moment from the second measurement by fitting the Breit-Rabi formula to the data presented in figure 4(b), where the only fit parameter was g_I . This is determined to be $f = 3199941076.89 \pm 0.02_{\text{stat}} \pm 0.13_{\text{syst}}$ Hz, which cor-

responds to a nuclear magnetic moment of $\mu_I/\mu_N = -1.315349(9)(4)$. The two uncertainties on the nuclear magnetic moment are due to the uncertainty in the ground-level hyperfine splitting E_{hfs} measured by Arbes *et al.*, and the uncertainty in our measurements respectively. Note that these measurements are not corrected for diamagnetic shielding of the nucleus due to the bound electrons [71, 72]. The two measurements are in excellent agreement with each other which gives confidence in the reported values given the differing spectroscopic methods and the nine month interval between measurements.

The measured nuclear magnetic moment μ_{meas} differs from that of the bare nucleus μ_{bare} because of diamagnetic shielding by the bound electrons. A calculation of the diamagnetic correction factor, $\mu_{\text{bare}}/\mu_{\text{meas}}$, for Ca^+ has not been published. However, there are published values for both Ca [57] and Ca^{2+} [58]. We approximate the correction for Ca^+ to be the mean of these values, and assume a 95% confidence interval between the Ca (1.001495) and Ca^{2+} (1.001465) correction factors, resulting in a diamagnetic correction of 1.001480(8) for Ca^+ . This is consistent with a recent unpublished calculation [73]. Applying this correction to our measurement, we calculate a corrected magnetic moment of $\mu_{\text{bare}}/\mu_N = -1.317297(13)$.

Our measurement (before diamagnetic correction) is consistent with previous measurements by Jeffries *et al.* [50] and Olschewski *et al.* [52], but disagrees with the precision NMR measurement by Lutz *et al.* [51] (see Table I). The measurement by Lutz *et al.* is, like our measurement, uncorrected for diamagnetic shielding due to the bound electrons. However, it is also uncorrected for the change in shielding constant due to the D_2O solution in which the Ca^{2+} ions were measured, to which we attribute the discrepancy [74]. Lutz *et al.* used the free-atom measurement of Olschewski *et al.* [52] to determine the shielding constant, defined as $\sigma = 1 - (\mu_{\text{meas}}/\mu_{\text{bare}})$.

However, the measurement by Olschewski *et al.* [52] does not have a diamagnetic correction applied, and therefore Lutz *et al.* were in fact measuring the change in shielding constant between a free atom and a solvated ion. We define this as $\Delta\sigma = \sigma_{\text{NMR}} - \sigma_{\text{atom}}$ where the subscripts refer to the measurement technique. Due to the large uncertainty in μ_{atom} , Lutz *et al.* reported a measurement of $\Delta\sigma = -0.0002(5)$ which is consistent with zero. With our precision measurement of μ_I we can evaluate the change in shielding constant between a free Ca^+ ion and a solvated Ca^{2+} ion to be $\Delta\sigma = -0.00022(1)$. By comparing the calculated shielding constant of Ca^{2+} in H_2O [58] and that estimated above for Ca^+ , we are able to extract a theoretical change of shielding constant of $\Delta\sigma = -0.00022(4)$, which is consistent with our measurements.

The precision of our nuclear magnetic moment measurement is limited by the uncertainty in the ground-level hyperfine splitting measured by Arbes *et al.* This measurement could be improved in the following way. The sensitivity of a hyperfine transition to μ_I is dominated by the second term of equation 2. Therefore, by applying the demonstrated techniques to a $\Delta M = 0$ transition, such as the $|F = 4, M = 1\rangle \rightarrow |F = 3, M = 1\rangle$ clock transition at $B = 287.783\text{ G}$, it would be possible to improve upon the current measurement of E_{hfs} and hence the overall precision of μ_I . To increase precision further, the size of

the RF-induced AC Zeeman shift could be reduced by performing the measurements in a 3D Paul trap with a symmetric trap design to minimize RF magnetic fields at the ion. With increased precision, it may be necessary to take into account modifications to the Breit-Rabi formula [75].

We note that these measurement techniques could also be applied to more exotic calcium isotopes with nuclear spin. For example, ^{41}Ca [76, 77] and ^{45}Ca can both be readily artificially produced, and have long enough half-lives to be used in similar experiments.

In summary, we have performed two precision measurements of the nuclear magnetic moment of a single $^{43}\text{Ca}^+$ trapped in a surface-electrode Paul trap. These measurements improve upon previous free-atom experiments [52] by more than one order-of-magnitude, and are free from systematic shifts associated with NMR measurements [50, 51]. This measurement adds to the increasing number of precision nuclear moment measurements, and improves the accuracy of measurements in the calcium isotopic chain which are critical in tests of fundamental physics theories.

We thank Derek Stacey and Andrej Antušek for helpful discussions. This work was supported by the U.S. Army Research Office (contract no. W911NF-18-1-0340) and UK EPSRC.

-
- [1] V. M. Shabaev, D. A. Glazov, G. Plunien, and A. V. Volotka. Theory of bound-electron g -factor in highly charged ions. *J. Phys. Chem. Ref. Data*, 44(3):031205, 2015.
- [2] B. Schabinger, S. Sturm, A. Wagner, J. Alonso, W. Quint, G. Werth, and K. Blaum. Experimental g -factor of hydrogen-like silicon-28. *Eur. Phys. J. D*, 66(3):71, 2012.
- [3] A. Wagner, S. Sturm, F. Köhler, D. A. Glazov, A. V. Volotka, G. Plunien, W. Quint, G. Werth, V. M. Shabaev, and K. Blaum. g -factor of lithium-like silicon $^{28}\text{Si}^{11+}$. *Phys. Rev. Lett.*, 110(3):033003, 2013.
- [4] S. Sturm, G. Werth, and K. Blaum. Electron g -factor determinations in Penning traps. *Ann. Phys.*, 525(8-9):620–635, 2013.
- [5] S. Sturm, M. Vogel, F. Köhler-Langes, W. Quint, K. Blaum, and G. Werth. High-precision measurements of the bound electron’s magnetic moment. *Atoms*, 5(1):4, 2017.
- [6] M. G. Kozlov, M. S. Safronova, J. R. Crespo López-Urrutia, and P. O. Schmidt. Highly charged ions: Optical clocks and applications in fundamental physics. *Rev. Mod. Phys.*, 90(4):045005, 2018.
- [7] P. Indelicato. QED tests with highly charged ions. *J. Phys. B: At. Mol. Opt. Phys.*, 52(23):232001, 2019.
- [8] R. Pohl, R. Gilman, G. A. Miller, and K. Pachucki. Muonic hydrogen and the proton radius puzzle. *Annu. Rev. Nucl. Part. S.*, 63:175–204, 2013.
- [9] C. E. Carlson. The proton radius puzzle. *Prog. Part. Nucl. Phys.*, 82:59–77, 2015.
- [10] H. W. Hammer and U. G. Meißner. The proton radius: from a puzzle to precision. *Sci. Bull.*, 65(4):257–258, 2020.
- [11] M. G. H. Gustavsson and A.-M. Mårtensson-Pendrill. Need for remeasurements of nuclear magnetic dipole moments. *Phys. Rev. A*, 58(5):3611, 1998.
- [12] V. M. Shabaev, M. Tomaselli, T. Kühn, A. N. Artemyev, and V. A. Yerokhin. Ground-state hyperfine splitting of high- Z hydrogen-like ions. *Phys. Rev. A.*, 56(1):252, 1997.
- [13] A. Bohr and V. F. Weisskopf. The influence of nuclear structure on the hyperfine structure of heavy elements. *Phys. Rev.*, 77(1):94, 1950.
- [14] S. Büttgenbach. Magnetic hyperfine anomalies. *Hyperfine Interact.*, 20(1):1–64, 1984.
- [15] J. Ullmann, Z. Andelkovic, C. Brandau, A. Dax, W. Geithner, C. Geppert, C. Gorges, M. Hammen, V. Hannen, S. Kaufmann, et al. High precision hyperfine measurements in bismuth challenge bound-state strong-field QED. *Nat. Comm.*, 8(1):1–7, 2017.
- [16] L. V. Skripnikov, S. Schmidt, J. Ullmann, C. Geppert, F. Kraus, B. Kresse, W. Nörtershäuser, A. F. Privalov, B. Scheibe, V. M. Shabaev, et al. New nuclear magnetic moment of ^{209}Bi : Resolving the bismuth hyperfine puzzle. *Phys. Rev. Lett.*, 120(9):093001, 2018.
- [17] B. A. Brown. The nuclear shell model towards the drip lines. *Prog. Part. Nucl. Phys.*, 47(2):517–599, 2001.
- [18] E. Caurier, G. Martinez-Pinedo, F. Nowacki, A. Poves, and A. P. Zuker. The shell model as a unified view of nuclear structure. *Rev. Mod. Phys.*, 77(2):427, 2005.

- [19] T. Otsuka, A. Gade, O. Sorlin, T. Suzuki, and Y. Utsuno. Evolution of shell structure in exotic nuclei. *Rev. Mod. Phys.*, 92(1):015002, 2020.
- [20] M. G. Mayer. On closed shells in nuclei. II. *Phys. Rev.*, 75(12):1969, 1949.
- [21] K. Rutz, M. Bender, P. G. Reinhard, J. A. Maruhn, and W. Greiner. Odd nuclei and single-particle spectra in the relativistic mean-field model. *Nuc. Phys. A*, 634(1-2):67–88, 1998.
- [22] B. K. Sahoo. Nuclear quadrupole moment of ^{43}Ca and hyperfine-structure studies of its singly charged ion. *Phys. Rev. A*, 80(1):012515, 2009.
- [23] J. D. Holt, T. Otsuka, A. Schwenk, and T. Suzuki. Three-body forces and shell structure in calcium isotopes. *J. Phys. G: Nucl. Partic.*, 39(8):085111, 2012.
- [24] G. Hagen, M. Hjorth-Jensen, G. R. Jansen, R. Machleidt, and T. Papenbrock. Evolution of shell structure in neutron-rich calcium isotopes. *Phys. Rev. Lett.*, 109(3):032502, 2012.
- [25] R. Roth, S. Binder, K. Vobig, A. Calci, J. Langhammer, and P. Navrátil. Medium-mass nuclei with normal-ordered chiral NN + 3N interactions. *Phys. Rev. Lett.*, 109(5):052501, 2012.
- [26] J. D. Holt, J. Menéndez, J. Simonis, and A. Schwenk. Three-nucleon forces and spectroscopy of neutron-rich calcium isotopes. *Phys. Rev. C*, 90(2):024312, 2014.
- [27] V. Somà, A. Cipollone, C. Barbieri, P. Navrátil, and T. Duguet. Chiral two- and three-nucleon forces along medium-mass isotope chains. *Phys. Rev. C*, 89(6):061301, 2014.
- [28] K. H. Speidel, S. Schielke, O. Kenn, J. Leske, D. Hohn, H. Hodde, J. Gerber, P. Maier-Komor, O. Zell, Y. Y. Sharon, et al. Nuclear structure of the stable even-A calcium isotopes based on new experiments and shell model calculations. *Phys. Rev. C*, 68(6):061302, 2003.
- [29] R. F. Garcia-Ruiz, M. L. Bissell, K. Blaum, N. Frömmgen, J. D. Hammen, M. and Holt, M. Kowalska, K. Kreim, J. Menéndez, R. Neugart, et al. Ground-state electromagnetic moments of calcium isotopes. *Physical Review C*, 91(4):041304, 2015.
- [30] F. Köhler, K. Blaum, M. Block, S. Chenmarev, S. Eliseev, D. A. Glazov, M. Goncharov, J. Hou, A. Kracke, D. A. Nesterenko, et al. Isotope dependence of the Zeeman effect in lithium-like calcium. *Nat. Comm.*, 7(1):1–8, 2016.
- [31] R. F. Garcia Ruiz, M. L. Bissell, K. Blaum, A. Ekström, N. Frömmgen, G. Hagen, M. Hammen, K. Hebel, J. D. Holt, G. R. Jansen, et al. Unexpectedly large charge radii of neutron-rich calcium isotopes. *Nat. Phys.*, 12(6):594–598, 2016.
- [32] A. Klose, K. Minamisono, A. J. Miller, B. A. Brown, D. Garand, J. D. Holt, J. D. Lantis, Y. Liu, B. Maaß, W. Nörtershäuser, et al. Ground-state electromagnetic moments of ^{37}Ca . *Phys. Rev. C*, 99(6):061301, 2019.
- [33] H. W. Hammer, A. Nogga, and A. Schwenk. Colloquium: Three-body forces: From cold atoms to nuclei. *Rev. Mod. Phys.*, 85(1):197, 2013.
- [34] A. Ozawa, T. Kobayashi, T. Suzuki, K. Yoshida, and I. Tanihata. New magic number, $N = 16$, near the neutron drip line. *Phys. Rev. Lett.*, 84(24):5493, 2000.
- [35] D. Steppenbeck, S. Takeuchi, N. Aoi, P. Doornenbal, M. Matsushita, H. Wang, H. Baba, N. Fukuda, M. Go, S. and Honma, et al. Evidence for a new nuclear ‘magic number’ from the level structure of ^{54}Ca . *Nature*, 502(7470):207–210, 2013.
- [36] F. Wienholtz, D. Beck, K. Blaum, Ch. Borgmann, M. Breitenfeldt, R. B. Cakirli, S. George, F. Herfurth, J. D. Holt, M. Kowalska, et al. Masses of exotic calcium isotopes pin down nuclear forces. *Nature*, 498(7454):346–349, 2013.
- [37] S. Michimasa, M. Kobayashi, Y. Kiyokawa, S. Ota, D. S. Ahn, H. Baba, G. P. A. Berg, M. Dozono, N. Fukuda, T. Furuno, et al. Magic nature of neutrons in ^{54}Ca : first mass measurements of $^{55-57}\text{Ca}$. *Phys. Rev. Lett.*, 121(2):022506, 2018.
- [38] A. Corney. *Atomic and laser spectroscopy*. Clarendon Press Oxford, 1978.
- [39] G. Breit and I. I. Rabi. Measurement of nuclear spin. *Phys. Rev.*, 38(11):2082, 1931.
- [40] E. Arimondo, M. Inguscio, and P. Violino. Experimental determinations of the hyperfine structure in the alkali atoms. *Rev. Mod. Phys.*, 49(1):31, 1977.
- [41] J. A. Pople. The theory of chemical shifts in nuclear magnetic resonance I. Induced current densities. *Proc. R. Soc. A*, 239(1219):541–549, 1957.
- [42] J. A. Pople. The theory of chemical shifts in nuclear magnetic resonance II. Interpretation of proton shifts. *Proc. R. Soc. A*, 239(1219):550–556, 1957.
- [43] M. Kaupp, M. Buhl, and V. G. Malkin. *Calculation of NMR and EPR Parameters*. Wiley Online Library, 2004.
- [44] G. Werth. Hyperfine structure and g -factor measurements in ion traps. *Phys. Scr.*, 1995(T59):206, 1995.
- [45] G. Savard and G. Werth. Precision nuclear measurements with ion traps. *Annu. Rev. Nuc. and Part. S.*, 50(1):119–152, 2000.
- [46] J. P. Karr. Precision measurements with non-laser-cooled trapped ions. *J. Phys. B: At. Mol. Opt. Phys.*, 42(15):154018, 2009.
- [47] F. Arbes, O. Becker, H. Knab, K. H. Knöll, and G. Werth. On the possible determination of hyperfine anomalies by trapped ion spectroscopy. *Nucl. Instr. Meth. B*, 70(1-4):494–499, 1992.
- [48] G. Tommaseo, T. Pfeil, G. Revalde, G. Werth, P. Indelicato, and J. P. Desclaux. The g_J -factor in the ground state of Ca^+ . *Eur. Phys. J. D*, 25(2):113–121, 2003.
- [49] G. Marx, G. Tommaseo, and G. Werth. Precise g_J - and g_I -factor measurements of Ba^+ isotopes. *Eur. Phys. J. D.*, 4(3):279–284, 1998.
- [50] C. D. Jeffries. The spin and magnetic moment of ^{43}Ca . *Phys. Rev.*, 90(6):1130, 1953.
- [51] O. Lutz, A. Schwenk, and A. Uhl. Nuclear magnetic resonance studies of ^{43}Ca . *Z. Naturforsch. A*, 28(9):1534–1536, 1973.
- [52] L. Olschewski. Messung der magnetischen Kerndipolmomente an freien ^{43}Ca -, ^{87}Sr -, ^{135}Ba -, ^{137}Ba -, ^{171}Yb - und ^{173}Yb -Atomen mit optischem Pumpen. *Z. Phys.*, 249(3):205–227, 1972.
- [53] D. T. C. Allcock, T. P. Harty, C. J. Ballance, B. C. Keitch, N. M. Linke, D. N. Stacey, and D. M. Lucas. A microfabricated ion trap with integrated microwave circuitry. *Appl. Phys. Lett.*, 102(4):044103, 2013.
- [54] N. F. Ramsey. A molecular beam resonance method with separated oscillating fields. *Phys. Rev.*, 78(6):695, 1950.
- [55] C. Langer, R. Ozeri, J. D. Jost, J. Chiaverini, B. DeMarco, A. Ben-Kish, R. B. Blakestad, J. Britton, D. B. Hume, W. M. Itano, et al. Long-lived qubit memory using atomic ions. *Phys. Rev. Lett.*, 95(6):060502, 2005.
- [56] T. P. Harty, D. T. C. Allcock, C. J. Ballance, L. Guidoni,

- H. A. Janacek, N. M. Linke, D. N. Stacey, and D. M. Lucas. High-fidelity preparation, gates, memory, and readout of a trapped-ion quantum bit. *Phys. Rev. Lett.*, 113(22):220501, 2014.
- [57] G. H. Fuller. Nuclear spins and moments. *J. Phys. Chem. Ref. Data*, 5(4):835–1092, 1976.
- [58] A. Antušek, P. Rodziewicz, D. Ke, A. Kaczmarek-Ke, M. Jaszuński, et al. Ab initio study of NMR shielding of alkali earth metal ions in water complexes and magnetic moments of alkali earth metal nuclei. *Chem. Phys. Lett.*, 588:57–62, 2013.
- [59] D. M. Lucas, A. Ramos, J. P. Home, M. J. McDonnell, S. Nakayama, J-P Stacey, S. C. Webster, D. N. Stacey, and A. M. Steane. Isotope-selective photoionization for calcium ion trapping. *Phys. Rev. A*, 69(1):012711, 2004.
- [60] Stanford Research Systems FS725.
- [61] Trimble Thunderbolt GPS-disciplined oscillator.
- [62] A. H. Myerson, D. J. Szwer, S. C. Webster, D. T. C. Allcock, M. J. Curtis, G. Imreh, J. A. Sherman, D. N. Stacey, A. M. Steane, and D. M. Lucas. High-fidelity readout of trapped-ion qubits. *Phys. Rev. Lett.*, 100(20):200502, 2008.
- [63] I. Hughes and T. Hase. *Measurements and their uncertainties: a practical guide to modern error analysis*. Oxford University Press, 2010.
- [64] D. J. Berkeland, J. D. Miller, J. C. Bergquist, W. M. Itano, and D. J. Wineland. Laser-cooled mercury ion frequency standard. *Phys. Rev. Lett.*, 80(10):2089, 1998.
- [65] D. T. C. Allcock. *Surface-electrode ion traps for scalable quantum computing*. PhD thesis, Oxford University, UK, 2011.
- [66] The gradients df/dE are independent of trap RF power P_{RF} : we measure the AC Zeeman shift to vary linearly for small displacements x of the ion, so that it is proportional to xP_{RF} , while $x \propto 1/P_{\text{RF}}$ for a given E .
- [67] T. P. Harty. *High-fidelity microwave-driven quantum logic in intermediate-field $^{43}\text{Ca}^+$* . PhD thesis, Oxford University, UK, 2013.
- [68] M. Sepiol. *A high-fidelity microwave driven two-qubit quantum logic gate in $^{43}\text{Ca}^+$* . PhD thesis, University of Oxford, 2016.
- [69] W. M. Itano, L. L. Lewis, and D. J. Wineland. Shift of $^2\text{S}_{1/2}$ hyperfine splittings due to blackbody radiation. *Phys. Rev. A*, 25(2):1233, 1982.
- [70] The radial thermal motion considered above will only slightly increase the rms RF field experienced by the ion.
- [71] W. E. Lamb Jr. Internal diamagnetic fields. *Phys. Rev.*, 60(11):817, 1941.
- [72] P. Pyykkö. Perspective on Norman Ramsey’s theories of NMR chemical shifts and nuclear spin-spin coupling. *Theor. Chem. Acc.*, 103(3-4):214–216, 2000.
- [73] A. Antušek. Personal communication. 2021.
- [74] We note that the differences in the diamagnetic shielding constants between Ca^+ and Ca^{2+} given above are an order of magnitude too small to explain the discrepancy.
- [75] N. Shiga, W. M. Itano, and J. J. Bollinger. Diamagnetic correction to the $^9\text{Be}^+$ ground-state hyperfine constant. *Phys. Rev. A*, 84(1):012510, 2011.
- [76] S. Hasegawa, L. Matsuoka, Y. Fukushima, H.i Osaki, and Y. Hashimoto. Development of ion trap technique for rare isotope measurement. *J. Nucl. Sci. Technol.*, 43(4):300–304, 2006.
- [77] M. Kitaoka, T. Yoshida, Y. Yamamoto, K. Jung, and S. Hasegawa. Trapping and laser cooling of trace Ca^+ isotopes injected from an inductively coupled plasma mass spectrometer. *J. Anal. At. Spectrom.*, 28(8):1292–1297, 2013.